Applied Mathematical Modelling 34 (2010) 3917–3932

Contents lists available at ScienceDirect

Applied Mathematical Modelling

journal homepage: www.elsevier.com/locate/apm

High dimensional model representation for stochastic finite element analysis

R. Chowdhury *, S. Adhikari

School of Engineering, Swansea University, Singleton Park, Swansea, SA2 8PP Wales, UK

ARTICLE INFO

Article history:
Received 12 January 2009
Received in revised form 31 March 2010
Accepted 6 April 2010
Available online 14 April 2010

Keywords:
Function approximation
High dimensional model representation
Karhunen–Loève expansion
Random field
Stochastic finite element

ABSTRACT

This paper presents a generic high dimensional model representation (HDMR) method for approximating the system response in terms of functions of lower dimensions. The proposed approach, which has been previously applied for problems dealing only with random variables, is extended in this paper for problems in which physical properties exhibit spatial random variation and may be modelled as random fields. The formulation of the extended HDMR is similar to the spectral stochastic finite element method in the sense that both of them utilize Karhunen–Loève expansion to represent the input, and lower-order expansion to represent the output. The method involves lower dimensional HDMR approximation of the system response, response surface generation of HDMR component functions, and Monte Carlo simulation. Each of the low order terms in HDMR is sub-dimensional, but they are not necessarily translating to low degree polynomials. It is an efficient formulation of the system response, if higher-order variable correlations are weak, allowing the physical model to be captured by the first few lower-order terms. Once the approximate form of the system response is defined, the failure probability can be obtained by statistical simulation. The proposed approach decouples the finite element computations and stochastic computations, and consecutively the finite element code can be treated as a black box, as in the case of a commercial software. Numerical examples are used to illustrate the features of the extended HDMR and to compare its performance with full scale simulation.

1. Introduction

Numerical methods for structural analysis have been developed quite substantially over the last decades. In particular, the finite element method (FEM) and closely related approximations have become state-of-the-art. The modelling capabilities and the solution possibilities lead to an increasing refinement allowing for more and more details to be captured in the analysis. On the other hand, however, the need for more precise input data becomes urgent in order to avoid or reduce possible modelling errors. Such errors could eventually render the entire analysis procedure useless. Typically, not all uncertainties encountered in structural analysis can be reduced by careful modelling since their source lies in the intrinsic randomness [1–3] of natural phenomena. It is therefore appropriate to utilize methods based on probability theory to assess such uncertainties and to quantify their effect on the outcome of structural analysis.

In the stochastic mechanics community, the need to account for uncertainties has long been recognized in order to achieve reliable design of structural and mechanical systems [4–6]. There is a general agreement that advanced computational tools have to be employed to provide the necessary computational framework for describing structural response

* Corresponding author. Tel.: +44 (0)1792 602088; fax: +44 (0)1792 295676.
E-mail address: R.Chowdhury@swansea.ac.uk (R. Chowdhury).

0307-904X/$ - see front matter © 2010 Elsevier Inc. All rights reserved.
doi:10.1016/j.apm.2010.04.004

and reliability. A current popular method is the stochastic finite element method (SFEM) [7], which integrates probability theory with standard FEM. Methods involving perturbation expansion [8], Neumann series expansion [9], first- and second-order reliability algorithms [10–12], and Monte Carlo simulation (MCS) [13] including variance reduction strategies have been developed and extensively used for probabilistic analysis of complex structures. These developments include treatment of spatially varying structural properties that are modelled as random fields, loads that are modelled as space–time random processes, structural behaviour covering static and dynamic regimes, linear and nonlinear structural/mechanical behaviour, characterization of response variability and determination of structural reliability measures. Early development of Spectral SFEM (SSFEM) by Ghanem and Spanos [7] appears to be a suitable technique for the solution of complex, general problems in probabilistic mechanics. However, this method requires access to the governing differential equations of system. Furthermore, the resulting system of equations to be solved for the unknown response is much larger than those from deterministic finite element analysis. For complicated large system problems, the system of equations in the SSFEM could be tremendously large. For example, if the deterministic system is of size $l \times l$, and the number of terms in the polynomial chaos expansion is p, then the size of the stochastic system would be $p \times l \times p \times l$. Recently a new implementation of SSFEM [14], which is theoretically equivalent to the original SSFEM, has been developed for the purpose of utilizing commonly available FEM codes as a black box. This novel implementation of SSFEM uses random sampling of the input and consequently a large number of FEM runs to get a stable estimate of the coefficients in the expansion of the solution.

This paper presents a generic approach for solving random field problems arising in structural mechanics. The methodology is based on high dimensional model representation (HDMR) which has been previously proposed by the authors [15–18] for problems dealing only with random variables. This paper extends HDMR concept to the problems involving random fields. Proposed methodology uses Karhunen–Loève (K–L) expansion [19] for discretizing the input random field and HDMR to approximate the output response in terms of functions of lower dimensions as an efficient uncertainty propagation model.

Compared to the conventional surrogate models, present approach has several advantages to justify using it as a more reliable metamodel. The first is reduction of data processing. The exponentially growing amount of function values is represented via polynomially growing tables [15,16] holding each function component (terms in the general expansion). This property helps us to cope with high dimensional problems of real world. The second advantage is reduction of computational complexity. HDMR is generated by a family of (linear) projections [20,21]. Consequently, it allows splitting of any problem into easier low-dimensional subproblems. Third advantage is that, HDMR is a mean square convergent series expansion. This is because of the inherent properties of orthogonal properties of HDMR component functions [20]. It is optimal in the Fourier sense since it minimizes the mean square error from truncation after a finite number of cooperative terms in the expansion. Also lower dimensional functions stay stable as higher order Taylor series terms are inherently included. Finally, compared to existing simulation based random field approach [22], HDMR-based approach does not translate into lower-order polynomial approximation of system response. The formulation of the extended HDMR is similar to the SSFEM in the sense that both of them utilize K–L expansion to represent the input, and lower-order expansion to represent the output. The sample points in the proposed method are chosen from regularly spaced points along each of the variable axis. This sampling scheme results in fewer system analysis [15,16].

Organization of the present paper is as follows. In Section 2, statement of the problem is set in the context of stochastic mechanics. Emphasis is put on explaining how to discretize the random field. Section 3 provides an overview of the theory behind the implementation of HDMR. Section 4 describes the step-wise procedure of HDMR-based metamodel. In Section 5, computational steps of the proposed approach are discussed. Numerical examples are illustrated in Section 6, to show the performance of the proposed approach.

2. Random field discretization

Let $(\Theta, \mathcal{F}, \mathcal{P})$ be a probability space and let $\mathcal{L}_2(\Theta, \mathcal{F}, \mathcal{P})$ be the Hilbert space of random variables with finite second moments. A random field $\mathcal{H}(\boldsymbol{x}, \theta)$ with $\boldsymbol{x} \in \Re^N$ and $\theta \in \Theta$, is curve in $\mathcal{L}_2(\Theta, \mathcal{F}, \mathcal{P})$, that is a collection of random variables indexed by $\boldsymbol{x}$ [23]. Hence, $\mathcal{H}(\boldsymbol{x}_0, \theta)$ for a given $\boldsymbol{x}_0$ is a random variable and $\mathcal{H}(\mathbf{x}, \theta_0)$ for a given θ_0 is a realization of the random field. A Gaussian random field is such that for any N, the vector $[\mathcal{H}(\boldsymbol{x}_1, \theta_0), \ldots, \mathcal{H}(\boldsymbol{x}_N, \theta_0)]^T$ is Gaussian. Moreover, it is homogeneous if its mean $\mu(\boldsymbol{x}, \theta_0)$ and variance $\sigma^2(\boldsymbol{x}, \theta_0)$ are constant and its autocorrelation coefficient $\rho(\boldsymbol{x}, \boldsymbol{x}')$ is a function of $\boldsymbol{x}$ and $\boldsymbol{x}'$ only. This autocorrelation function may take many distinct forms. One such form is the exponential type

$$\rho(\boldsymbol{x}, \boldsymbol{x}') = \mathrm{e}^{-\alpha_1 |\boldsymbol{x}_{(1)} - \boldsymbol{x}'_{(1)}| - \alpha_2 |\boldsymbol{x}_{(2)} - \boldsymbol{x}'_{(2)}|} \tag{1}$$

where $\boldsymbol{x}_{(i)}$ denotes ith coordinate of $\boldsymbol{x}$ and α_1, α_2 are known as correlation lengths.

Random fields are a useful tool to model random mechanical properties of engineering systems which are spatially distributed in nature. This includes Poisson's ratio, Young's modulus and yield stress. It is well known that, for a linear system, the FEM eventually yields a system of algebraic equations of the form

$$\boldsymbol{K}\boldsymbol{u} = \boldsymbol{f}, \tag{2}$$

where $\boldsymbol{K} \in \Re^{N \times N}$ is known as stiffness matrix and $\boldsymbol{f} \in \Re^N$ is the force vector. If the uncertainty is taken into account, $\boldsymbol{K}$ becomes a random matrix.

Suppose one is interested in quantifying the uncertainty in Eq. (2) induced by the random properties in the system. When implementing the deterministic FEM, functions are represented by a set of parameters, that is, the values of the function and its derivatives at the nodal points. In the case of the SFEM, each random field involved is discretized by representing it as a set of random variables. Therefore, $\mathcal{H}(\boldsymbol{x},\theta)$ needs to be discretized in order to obtain the associated system of random algebraic equations. The solution to these equations will enable uncertainty quantification for the particular system in concern. A wide variety of discretization schemes are available in the literature. The discretization methods can be divided into three groups: point discretization (e.g., midpoint method [24], shape function method [8,25], integration point method [26], optimal linear estimate method [27]); average discretization method (e.g., spatial average [28,29], weighted integral method [30–33]) and series expansion method (e.g., Karhunen–Loève expansion [28], orthogonal series expansion [34], expansion optimal linear estimation [29]). An advantageous alternative for discretizing $\mathcal{H}(\boldsymbol{x},\theta)$ is the K–L expansion, for which

$$\mathcal{H}(\boldsymbol{x},\theta) = \sum_{i=1}^{\infty} \sqrt{\lambda_i}\xi_i(\theta)\psi_i(\boldsymbol{x}), \tag{3}$$

where $\{\xi_i(\theta)\}$ is a set of uncorrelated random variables, $\{\lambda_i\}$ is a set of constants and $\{\psi_i(\boldsymbol{x})\}$ is an orthogonal set of deterministic functions. In particular, $\{\lambda_i\}$ and $\{\psi_i(\boldsymbol{x})\}$ are the eigenvalues and eigenfunctions of the covariance kernel

$$\Gamma_{\mathcal{H}}(\boldsymbol{s}) \equiv \mathcal{E}[\mathcal{H}(\boldsymbol{x},\theta)\mathcal{H}(\boldsymbol{x}+\boldsymbol{s},\theta)] \equiv \Gamma_{\mathcal{H}}(\boldsymbol{x}_1,\boldsymbol{x}_2), \tag{4}$$

where $\boldsymbol{x}_1 = \boldsymbol{x}$, $\boldsymbol{x}_2 = \boldsymbol{x} + \boldsymbol{s}$, that is they arises from the solution of the integral equation

$$\int_{\mathfrak{R}^N} \Gamma_{\mathcal{H}}(\boldsymbol{x}_1,\boldsymbol{x}_2)\psi_i(\boldsymbol{x}_1)d\boldsymbol{x}_1 = \lambda_i\psi_i(\boldsymbol{x}_2). \tag{5}$$

The eigenfunctions are orthogonal in the sense that

$$\int_{\mathfrak{R}^N} \psi_i(\boldsymbol{x})\psi_j(\boldsymbol{x})d\boldsymbol{x} = \delta_{ij}, \tag{6}$$

where δ_{ij} is the Kronecker-delta function. In practice, the infinite series of Eq. (3) must be truncated, yielding a truncated K–L approximation

$$\mathcal{H}(\boldsymbol{x},\theta) \cong \bar{\mathcal{H}}(\boldsymbol{x}) + \sum_{i=1}^{M} \sqrt{\lambda_i}\xi_i(\theta)f_i(\boldsymbol{x}), \tag{7}$$

which approaches $\mathcal{H}(\boldsymbol{x},\theta)$ in the mean square sense as the positive integer $M \to \infty$. Finite element methods can be readily applied to obtain eigensolutions of any covariance function and domain of the random field. For linear or exponential covariance functions and simple domains, the eigensolutions can be evaluated analytically.

Once $\Gamma_{\mathcal{H}}(\boldsymbol{s})$ and its eigensolutions are determined, the parameterization of $\tilde{\mathcal{H}}(\boldsymbol{x},\theta)$ is achieved by the K–L approximation of its Gaussian image, i.e.,

$$\tilde{\mathcal{H}}(\boldsymbol{x},\theta) \cong G\left[\bar{\mathcal{H}}(\boldsymbol{x}) + \sum_{i=1}^{M} \sqrt{\lambda_i}\xi_i(\theta)f_i(\boldsymbol{x})\right]. \tag{8}$$

According to Eq. (8), the K–L approximation provides a parametric representation of the $\tilde{\mathcal{H}}(\boldsymbol{x},\theta)$ and, hence, of $\tilde{\mathcal{H}}(\boldsymbol{x},\theta)$ with M random variables. Note that this is not the only available technique to discretize the random field $\mathcal{H}(\boldsymbol{x},\theta)$. The K–L expansion has uniqueness and error-minimization properties that make it a convenient choice over other available methods. See [35] for a detailed study of the cited and other K–L expansion properties.

Engineers are interested in obtaining the probability density function and the cumulative distribution function of $\boldsymbol{u}$ in order to assess the reliability of the system. However, this objective can prove to be difficult to achieve and the approach is limited to obtaining the first few statistical moments of $\boldsymbol{u}$. There exist several strategies, such as perturbation and projection methods, to deal with this problem. An account of these methods is given in [36].

3. A brief overview of HDMR

The fundamental principle underlying the HDMR [20,21,37,38] is that, from the perspective of the output/response, the order of the functional correlations between the statistically independent variables will die off rapidly. This assertion does not eliminate strong variable dependence or even the possibility that all the variables are important. Various sources [20,37] of information support the fact that the high-order correlations are limited. First, the variables in most systems are chosen to enter as independent entities. Second, traditional statistical analyses of system behaviour have revealed that a variance and covariance analysis of the output in relation to the input variables often adequately describes the physics of the problem. These general observations lead to a dramatically reduced computational scaling when one seeks to map input–output relationships of complex systems.

Evaluating the input–output mapping of the system generates a HDMR. This is achieved by expressing system response as a hierarchical, correlated function expansion of a mathematical structure and evaluating each term of the expansion

independently. One may show that system response $g(\boldsymbol{x}) = g(x_1, x_2, \ldots, x_N)$ can be expressed as summands of different dimensions:

$$g(\boldsymbol{x}) = g_0 + \sum_{i=1}^{N} g_i(x_i) + \sum_{1 \leqslant i_1 < i_2 \leqslant N} g_{i_1 i_2}(x_{i_1}, x_{i_2}) + \cdots + \sum_{1 \leqslant i_1 < \cdots < i_l \leqslant N} g_{i_1 i_2 \cdots i_l}(x_{i_1}, x_{i_2}, \ldots, x_{i_l}) + \cdots + g_{12\cdots N}(x_1, x_2, \ldots, x_N), \tag{9}$$

where g_0 is a constant term representing the mean response of $g(\boldsymbol{x})$. The function $g_i(x_i)$ describes the independent effect of variable x_i acting alone, although generally nonlinearly, upon the output $g(\boldsymbol{x})$. The function $g_{i_1 i_2}(x_{i_1}, x_{i_2})$ gives pair cooperative effect of the variables x_{i_1} and x_{i_2} upon the output $g(\boldsymbol{x})$. The last term $g_{12\cdots N}(x_1, x_2, \ldots, x_N)$ contains any residual correlated behaviour over all of the system variables. Usually the higher order terms in Eq. (9) are negligible [21] such that HDMR with only low order correlations to second-order [38], amongst the input variables are typically adequate in describing the output behaviour.

The expansion functions are determined by evaluating the input–output responses of the system relative to the defined reference point $\bar{\boldsymbol{x}} = \{\bar{x}_1, \bar{x}_2, \ldots, \bar{x}_N\}$ along associated lines, surfaces, subvolumes, etc. (i.e. cuts) in the input variable space. This process reduces to the following relationship for the component functions in Eq. (9)

$$g_0 = g(\bar{\boldsymbol{x}}), \tag{10}$$

$$g_i(x_i) = g(x_i, \bar{\boldsymbol{x}}^i) - g_0, \tag{11}$$

$$g_{i_1 i_2}(x_{i_1}, x_{i_2}) = g(x_{i_1}, x_{i_2}, \bar{\boldsymbol{x}}^{i_1 i_2}) - g_{i_1}(x_{i_1}) - g_{i_2}(x_{i_2}) - g_0, \tag{12}$$

where the notation $g(x_i, \bar{\boldsymbol{x}}^i) = g(\bar{x}_1, \bar{x}_2, \ldots, \bar{x}_{i-1}, x_i, \bar{x}_{i+1}, \ldots, \bar{x}_N)$ denotes that all the input variables are at their reference point values except x_i. The g_0 term is the output response of the system evaluated at the reference point $\bar{\boldsymbol{x}}$. The higher order terms are evaluated as cuts in the input variable space through the reference point. Therefore, each first-order term $g_i(x_i)$ is evaluated along its variable axis through the reference point. Each second-order term $g_{i_1 i_2}(x_{i_1}, x_{i_2})$ is evaluated in a plane defined by the binary set of input variables x_{i_1}, x_{i_2} through the reference point, etc. The process of subtracting off the lower-order expansion functions removes their dependence to assure a unique contribution from the new expansion function.

Considering terms up to first- and second-order in Eq. (9) yields, respectively

$$g(\boldsymbol{x}) = g_0 + \sum_{i=1}^{N} g_i(x_i) + \mathcal{R}_2 \tag{13}$$

and

$$g(\boldsymbol{x}) = g_0 + \sum_{i=1}^{N} g_i(x_i) + \sum_{1 \leqslant i_1 < i_2 \leqslant N} g_{i_1 i_2}(x_{i_1}, x_{i_2}) + \mathcal{R}_3. \tag{14}$$

Substituting Eqs. (10)–(12) into Eqs. (13) and (14) leads to

$$g(\boldsymbol{x}) = \sum_{i=1}^{N} g(\bar{x}_1, \ldots, \bar{x}_{i-1}, x_i, \bar{x}_{i+1}, \ldots, \bar{x}_N) - (N-1) g(\bar{\boldsymbol{x}}) + \mathcal{R}_2 \tag{15}$$

and

$$\begin{aligned} g(\boldsymbol{x}) = {} & \sum_{\substack{i_1=1, i_2=1 \\ i_1 < i_2}}^{N} g(\bar{x}_1, \ldots, \bar{x}_{i_1-1}, x_{i_1}, \bar{x}_{i_1+1}, \ldots, \bar{x}_{i_2-1}, x_{i_2}, \bar{x}_{i_2+1}, \ldots, \bar{x}_N) - (N-2) \sum_{i=1}^{N} g(\bar{x}_1, \ldots, \bar{x}_{i-1}, x_i, \bar{x}_{i+1}, \ldots, \bar{x}_N) \\ & + \frac{(N-1)(N-2)}{2} g(\bar{\boldsymbol{x}}) + \mathcal{R}_3. \end{aligned} \tag{16}$$

Now consider first- and second-order approximation of $g(\boldsymbol{x})$, denoted respectively by

$$\tilde{g}(\boldsymbol{x}) \equiv g(x_1, x_2, \ldots, x_N) = \sum_{i=1}^{N} g(\bar{x}_1, \ldots, \bar{x}_{i-1}, x_i, \bar{x}_{i+1}, \ldots, \bar{x}_N) - (N-1) g(\bar{\boldsymbol{x}}) \tag{17}$$

and

$$\begin{aligned} \tilde{g}(\boldsymbol{x}) \equiv {} & g(x_1, x_2, \ldots, x_N) \\ = {} & \sum_{\substack{i_1=1, i_2=1 \\ i_1 < i_2}}^{N} g(\bar{x}_1, \ldots, \bar{x}_{i_1-1}, x_{i_1}, \bar{x}_{i_1+1}, \ldots, \bar{x}_{i_2-1}, x_{i_2}, \bar{x}_{i_2+1}, \ldots, \bar{x}_N) - (N-2) \sum_{i=1}^{N} g(\bar{x}_1, \ldots, \bar{x}_{i-1}, x_i, \bar{x}_{i+1}, \ldots, \bar{x}_N) \\ & + \frac{(N-1)(N-2)}{2} g(\bar{\boldsymbol{x}}). \end{aligned} \tag{18}$$

Comparison of Eqs. (15) and (17) indicates that the first-order approximation leads to the residual error $g(\boldsymbol{x}) - \tilde{g}(\boldsymbol{x}) = \mathcal{R}_2$, which includes contributions from terms of two and higher order component functions. Similarly the second-order approximation leads to the residual error $g(\boldsymbol{x}) - \tilde{g}(\boldsymbol{x}) = \mathcal{R}_3$, which includes contributions from terms of three and higher order component functions.

The notion of 0th, 1st, 2nd order, etc., in HDMR expansion should not be confused with the terminology used either in the Taylor series or in the conventional least-squares based metamodel. It can be shown that, the first-order component function $g_i(x_i)$ is the sum of all the Taylor series terms which contain and only contain variable x_i. Similarly, the second-order component function $g_{i_1 i_2}(x_{i_1}, x_{i_2})$ is the sum of all the Taylor series terms which contain and only contain variables x_{i_1} and x_{i_2}. Hence first- and second-order HDMR approximations should not be viewed as first- or second-order Taylor series expansions nor do they limit the nonlinearity of $g(\boldsymbol{x})$. Furthermore, the approximations contain contributions from all input variables. Thus, the infinite number of terms in the Taylor series are partitioned into finite different groups and each group corresponds to one cut-HDMR component function. Therefore, any truncated cut-HDMR expansion provides a better approximation and convergent solution of $g(\boldsymbol{x})$ than any truncated Taylor series because the latter only contains a finite number of terms of Taylor series. Furthermore, the coefficients associated with higher dimensional terms are usually much smaller than that with one-dimensional terms. As such, the impact of higher dimensional terms on the function is less, and therefore, can be neglected. If first-order HDMR approximation is not sufficient second-order HDMR approximation may be adopted at the expense of additional computational cost.

4. Construction of HDMR-based metamodel

HDMR in Eq. (9) is exact along any of the cuts and the output response $g(\boldsymbol{x})$ at a point $\boldsymbol{x}$ off of the cuts can be obtained by following the procedure in step 1 and step 2 below:

Step 1: Interpolate each of the low-dimensional HDMR expansion terms with respect to the input values of the point $\boldsymbol{x}$. For example, consider the first-order component function $g(x_i, \bar{\boldsymbol{x}}^i) = g(\bar{x}_1, \bar{x}_2, \ldots, \bar{x}_{i-1}, x_i, \bar{x}_{i+1}, \ldots, \bar{x}_N)$. If for $x_i = x_i^j$, n function values

$$g(x_i^j, \bar{\boldsymbol{x}}^i) = g(\bar{x}_1, \ldots, \bar{x}_{i-1}, x_i^j, \bar{x}_{i+1}, \ldots, \bar{x}_N); \quad j = 1, 2, \ldots, n \tag{19}$$

are given at n (=3, 5, 7 or 9) regularly spaced sample points along the variable axis x_i. The function value for arbitrary x_i can be obtained by the moving least-squares (MLS) interpolation [39] as

$$g(x_i, \bar{\boldsymbol{x}}^i) = \sum_{j=1}^{n} \phi_j(x_i) g'(\bar{x}_1, \ldots, \bar{x}_{i-1}, x_i^j, \bar{x}_{i+1}, \ldots, \bar{x}_N), \tag{20}$$

where

$$\begin{Bmatrix} g'(x_i^1, \boldsymbol{c}^i) \\ \vdots \\ \vdots \\ g'(x_i^n, \boldsymbol{c}^i) \end{Bmatrix} = \begin{bmatrix} \phi_1(x_i^1) & \phi_2(x_i^1) & \cdots & \phi_n(x_i^1) \\ \vdots & \vdots & \vdots & \vdots \\ \phi_1(x_i^n) & \phi_2(x_i^n) & \cdots & \phi_n(x_i^n) \end{bmatrix}^{-1} \begin{Bmatrix} g(x_i^1, \boldsymbol{c}^i) \\ \vdots \\ \vdots \\ g(x_i^n, \boldsymbol{c}^i) \end{Bmatrix}. \tag{21}$$

Similarly, consider the second-order component function $g(x_{i_1}, x_{i_2}, \bar{\boldsymbol{x}}^{i_1 i_2}) = g(\bar{x}_1, \ldots, \bar{x}_{i_1-1}, x_{i_1}, \bar{x}_{i_1+1}, \ldots, \bar{x}_{i_2-1}, x_{i_2}, \bar{x}_{i_2+1}, \ldots, \bar{x}_N)$. If for $x_{i_1} = x_{i_1}^{j_1}$, and $x_{i_2} = x_{i_2}^{j_2}$, n^2 function values

$$g(x_{i_1}^{j_1}, x_{i_2}^{j_2}, \bar{\boldsymbol{x}}^{i_1 i_2}) = g(\bar{x}_1, \ldots, \bar{x}_{i_1-1}, x_{i_1}^{j_1}, \bar{x}_{i_1+1}, \ldots, \bar{x}_{i_2-1}, x_{i_2}^{j_2}, \bar{x}_{i_2+1}, \ldots, \bar{x}_N); \quad j_1 = 1, 2, \ldots, n,\ j_2 = 1, 2, \ldots, n \tag{22}$$

are given on a grid formed by taking n (=3, 5, 7 or 9) regularly spaced sample points along x_{i_1} axis and x_{i_2} axis. The function value for arbitrary (x_{i_1}, x_{i_2}) can be obtained by the MLS interpolation [39] as

$$g(x_{i_1}, x_{i_2}, \bar{\boldsymbol{x}}^{i_1 i_2}) = \sum_{j_1=1}^{n} \sum_{j_2=1}^{n} \phi_{j_1 j_2}(x_{i_1}, x_{i_2}) g'(\bar{x}_1, \ldots, \bar{x}_{i_1-1}, x_{i_1}^{j_1}, \bar{x}_{i_1+1}, \ldots, \bar{x}_{i_2-1}, x_{i_2}^{j_2}, \bar{x}_{i_2+1}, \ldots, \bar{x}_N), \tag{23}$$

where

$$\begin{Bmatrix} g'(x_{i_1}^1, x_{i_2}^1, \boldsymbol{c}^{i_1 i_2}) \\ \vdots \\ g'(x_{i_1}^1, x_{i_2}^n, \boldsymbol{c}^{i_1 i_2}) \\ \vdots \\ g'(x_{i_1}^n, x_{i_2}^n, \boldsymbol{c}^{i_1 i_2}) \end{Bmatrix} = \begin{bmatrix} \phi_{11}(x_{i_1}^1, x_{i_2}^1) & \cdots & \phi_{1n}(x_{i_1}^1, x_{i_2}^1) & \cdots & \phi_{nn}(x_{i_1}^1, x_{i_2}^1) \\ \vdots & \vdots & \vdots & \vdots & \vdots \\ \phi_{11}(x_{i_1}^1, x_{i_2}^n) & \cdots & \phi_{1n}(x_{i_1}^1, x_{i_2}^n) & \cdots & \phi_{nn}(x_{i_1}^1, x_{i_2}^n) \\ \vdots & \vdots & \vdots & \vdots & \vdots \\ \phi_{11}(x_{i_1}^n, x_{i_2}^n) & \cdots & \phi_{1n}(x_{i_1}^n, x_{i_2}^n) & \cdots & \phi_{nn}(x_{i_1}^n, x_{i_2}^n) \end{bmatrix}^{-1} \begin{Bmatrix} g(x_{i_1}^1, x_{i_2}^1, \boldsymbol{c}^{i_1 i_2}) \\ \vdots \\ g(x_{i_1}^1, x_{i_2}^n, \boldsymbol{c}^{i_1 i_2}) \\ \vdots \\ g(x_{i_1}^n, x_{i_2}^n, \boldsymbol{c}^{i_1 i_2}) \end{Bmatrix}, \tag{24}$$

where the interpolation functions $\phi_j(x_i)$ and $\phi_{j_1 j_2}(x_{i_1}, x_{i_2})$ can be obtained using the MLS interpolation scheme [39].

By using Eq. (20), $g_i(x_i)$ can be generated if n function values are given at corresponding sample points. Similarly, by using Eq. (23), $g_{i_1 i_2}(x_{i_1}, x_{i_2})$ can be generated if n^2 function values at corresponding sample points are given. The same procedure shall be repeated for all the first-order component functions, i.e., $g_i(x_i);\ i = 1, 2, \ldots, N$ and the second-order component functions, i.e., $g_{i_1 i_2}(x_{i_1}, x_{i_2});\ i_1, i_2 = 1, 2, \ldots, N$.

Step 2: Sum the interpolated values of HDMR expansion terms from zeroth-order to the highest order retained in keeping with the desired accuracy. This leads to first-order HDMR approximation of the function $g(\boldsymbol{x})$ as

$$\tilde{g}(\boldsymbol{x}) = \sum_{i=1}^{N} \sum_{j=1}^{n} \phi_j(x_i) g'(\bar{x}_1, \ldots, \bar{x}_{i-1}, x_i^j, \bar{x}_{i+1}, \ldots, \bar{x}_N) - (N-1) g_0 \tag{25}$$

and second-order HDMR approximation of the function $g(\boldsymbol{x})$ as

$$\begin{aligned} \tilde{g}(\boldsymbol{x}) = & \sum_{\substack{i_1=1, i_2=1 \\ i_1<i_2}}^{N} \sum_{j_1=1}^{n} \sum_{j_2=1}^{n} \phi_{j_1 j_2}(x_{i_1}, x_{i_2}) g'(\bar{x}_1, \ldots, \bar{x}_{i_1-1}, x_{i_1}^{j_1}, \bar{x}_{i_1+1}, \ldots, \bar{x}_{i_2-1}, x_{i_2}^{j_2}, \bar{x}_{i_2+1}, \ldots, \bar{x}_N) - (N-2) \sum_{i=1}^{N} \\ & \times \sum_{j=1}^{n} \phi_j(x_i) g'(\bar{x}_1, \ldots, \bar{x}_{i-1}, x_i^j, \bar{x}_{i+1}, \ldots, \bar{x}_N) + \frac{(N-1)(N-2)}{2} g_0. \end{aligned} \tag{26}$$

5. Computational flow and effort

Computational flow of the proposed approach is presented in Fig. 1. A general procedure of HDMR for random field problems is briefly summarized below:

(i) Representation of random field inputs in terms of standard random variables by Karhunen–Loève expansion.
(ii) Once the inputs are expressed as functions of the selected standard random variables, the output quantities can also be represented as functions of the same set of standard random variables.
(iii) The model outputs are computed at a set of selected sample points and used to estimate the HDMR coefficients.
(iv) Calculation of the statistics of the output which are cast as a metamodel in terms of HDMR expansion. The statistics of the response can be estimated with the metamodel using either Monte Carlo simulation or analytical approximation.

6. Numerical examples

The implementation of the proposed approach is illustrated with the help of three examples in this section, involving one-dimensional and two-dimensional random fields. When comparing computational efforts in evaluating the statistics of responses, the number of actual finite element (FE) analysis is chosen as the primary comparison tool in this paper. This is because of the fact that, number of FE analysis indirectly indicates the CPU time usage. For full scale MCS, number of original FE analysis is same as the sampling size. While evaluating the statistics of responses through full scale MCS, CPU time is more because it involves number of repeated FE analysis. However, in the present methods MCS is conducted in conjunction with HDMR-based metamodel. Here, although the same sampling size as in direct MCS is considered, the number of FE analysis is much less. Hence, the computational effort expressed in terms of FE calculation alone should be carefully interpreted. A flow diagram of HDMR approximation is shown in Fig. 1. For first-order HDMR, n regularly spaced sample points are deployed along the variable axis through the reference point. Sampling scheme for first-order HDMR approximation of a function having one variable (x) and two variables (x_1 and x_2) is shown in Fig. 2(a) and (b), respectively. For second-order HDMR, n regularly spaced sample points are deployed along each of the variable axis to form a regular grid. Sampling scheme for second-order HDMR approximation of a function having two variables (x_1 and x_2) is shown in Fig. 3. In all numerical examples presented, the reference point $\bar{\boldsymbol{x}}$ is taken as mean values of the random variables. Since first- and second-order HDMR approximation leads to explicit representation of the system responses, the MCS can be conducted for any sampling size. The total cost of original FE analysis entails a maximum of $(n-1) \times N + 1$ and $(n-1)^2(N-1)N/2 + (n-1)N + 1$ by the present method using first- and second-order HDMR approximation, respectively.

6.1. Beam problem

A cantilever beam subjected to a concentrated load P (Fig. 4) is considered. It is assumed that the elastic modulus $E(\xi) = c_1 \exp[\alpha(\xi)]$ and thickness of the beam $t(\xi) = c_2 \exp[\beta(\xi)]$, which are spatially varying in the longitudinal direction, of the beam is an independent, homogeneous, lognormal random field. Mean and coefficient of variations of the random fields are $\mu_E = 2.07 \times 10^{11}\ \mathrm{N/m^2}$, $\mu_t = 0.254\ \mathrm{m}$; and $\upsilon_E = 0.4$, $\upsilon_t = 0.2$, respectively. $c_1 = \mu_E/\sqrt{1+\upsilon_E^2}$, $c_2 = \mu_t/\sqrt{1+\upsilon_t^2}$ and $\alpha(\xi)$, $\beta(\xi)$ are zero-mean, homogeneous, Gaussian random field with variance $\sigma_\alpha^2 = \ln(1+\upsilon_E^2)$; $\sigma_\beta^2 = \ln(1+\upsilon_t^2)$ and covariance function $\Gamma_\alpha(\xi_1, \xi_2) = \sigma_\alpha^2 \exp(-|\xi_1 - \xi_2|/b)$; $\Gamma_\beta(\xi_1, \xi_2) = \sigma_\beta^2 \exp(-|\xi_1 - \xi_2|/b)$. b is the correlation parameter that controls the rate at which the covariance decays. The degree of variability associated with the random process can be related

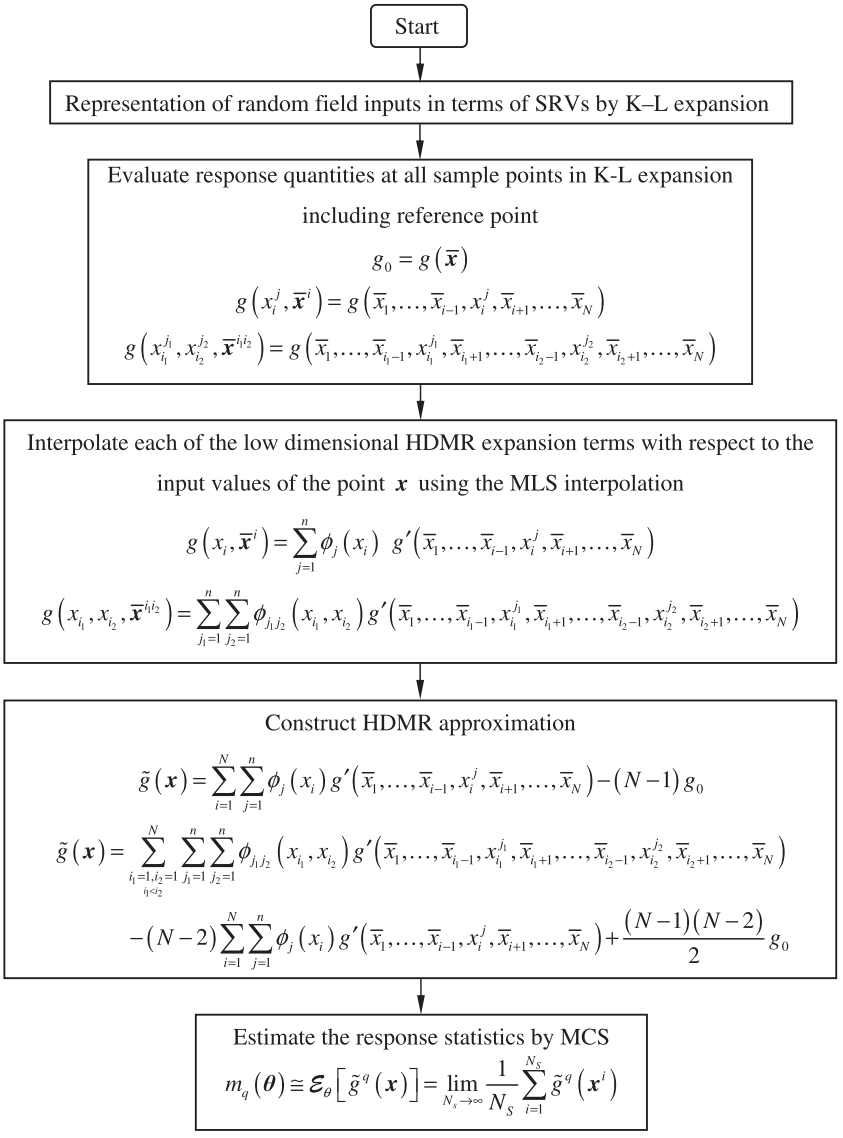

Fig. 1. Flowchart of HDMR-based stochastic FE analysis.

to its coefficient of variation. The frequency content of the random field is related to the L/b ratio in which L is the length of the beam. A small L/b ratio implies a highly correlated random field. $L/b = 1$ is chosen in this study. In this example, the length of the beam is $L = 1$ and it is divided into 10 elements.

The eigensolutions of the covariance function are obtained by solving the integral equation (Eq. (5)) analytically. The eigenvalues and eigenfunctions are given as follows:

$$
\begin{aligned}
\lambda_i &= \frac{2\sigma_\alpha^2 b}{\omega_i^2 + b^2}, \\
\lambda_i^* &= \frac{2\sigma_\alpha^2 b}{\omega_i^{*2} + b^2}, \\
\psi_i(\xi) &= \frac{\cos(\omega_i \xi)}{\sqrt{a + \frac{\sin(2\omega_i \xi)}{2\omega_i}}} \quad \text{for } i = \text{odd}, \\
\psi_i(\xi) &= \frac{\sin(\omega_i^* \xi)}{\sqrt{a - \frac{\sin(2\omega_i^* \xi)}{2\omega_i^*}}} \quad \text{for } i = \text{even}.
\end{aligned}
\tag{27}
$$

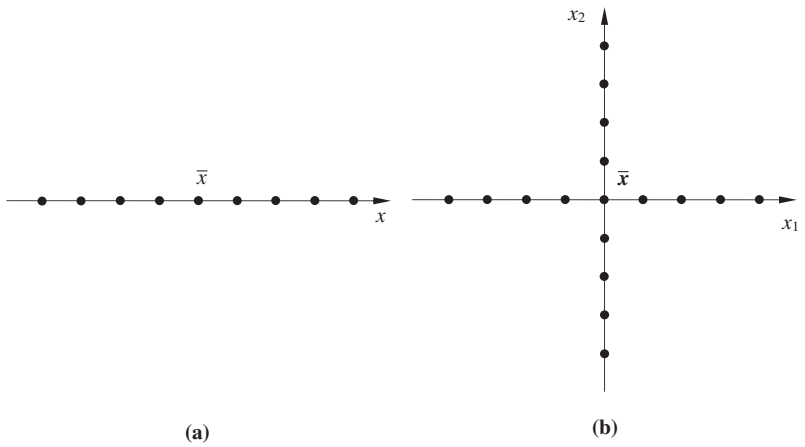

Fig. 2. Sampling scheme for first-order HDMR; (a) for a function having one variable (x); and (b) for a function having two variables (x_1 and x_2).

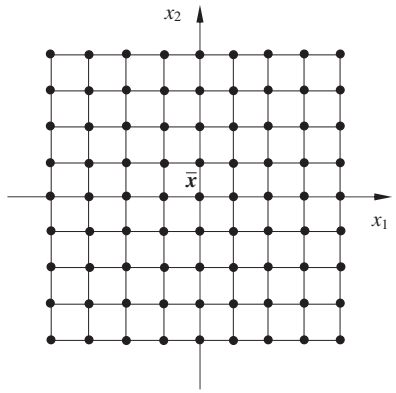

Fig. 3. Sampling scheme for second-order HDMR for a function having two variables (x_1 and x_2).

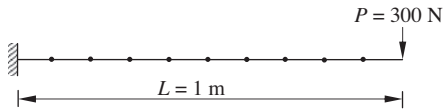

Fig. 4. Cantilever beam.

The random field is discretized into ten SRVs, and the 10-term K–L expansion (Eq. (7)) is used to generate sample functions of the input random field. The response quantity which is the tip displacement of the beam is represented by HDMR expansion with five sample points. To evaluate the validity of the results obtained from the proposed method full scale MCS is performed for the same problem. Realizations of the elastic modulus of the beam are numerically simulated using the K–L expansion method. For each of the realizations, the deterministic problem is solved and the statistics of the response are obtained. Fig. 4 compares the probability density functions obtained from first- and second-order HDMR with full scale MCS. Excellent agreements are observed between the proposed approach and 1×10^4 full scale MCS results. The cumulative distribution function is shown in Fig. 5.

Compared with the first two response moments obtained using direct MCS ($m_1 = 3.778 \times 10^{-2}$, $m_2 = 7.690 \times 10^{-3}$), present method using first-order HDMR approximation, underestimates the first two moments by 0.27% ($m_1 = 3.768 \times 10^{-2}$) and 1.41% ($m_2 = 7.582 \times 10^{-3}$), respectively, while second-order HDMR approximation, underestimates the first two moments by 0.02% ($m_1 = 3.777 \times 10^{-2}$) and 0.47% ($m_2 = 7.654 \times 10^{-3}$), respectively. The present method using first- and second-order HDMR approximation needs 41 and 761 original FE analysis, respectively, while full scale MCS requires 1×10^4 number of original FE calculation. This shows the accuracy and the efficiency (in terms of FE analysis) of the present method using first-order HDMR approximation, direct MCS.

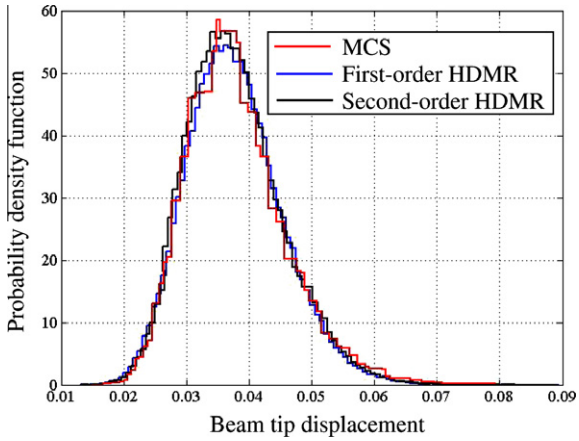

Fig. 5. Probability density function for beam tip displacement.

According to Huang et al. [40], K–L expansion with few terms (e.g., $M < 10$) do not yield accurate representation of the input random field (even for a highly correlated field, e.g. $L/b = 1$). It has also been shown that for a random field with $L/b = 1$, a two term representation may rise up to 30% error in the variance of the discretized field [28]. However, increasing the number of terms result in a large number of FE runs. Therefore, to balance between accuracy of the results and computational cost, $M = 10$ is considered in the present study. As the same random field discretization is used for full scale MCS and HDMR, the inaccuracy in input random field does not show in the results. However, the purpose of this paper is to show that HDMR can work as well as full scale MCS with much less FE runs. The inaccuracy in input random field for both methods is acknowledged Fig. 6.

6.2. Modal analysis of a fixed cantilever plate

This example involves the estimation of statistics of natural frequencies of a vibrating fixed cantilever plate with length $L_y = 1$ m and width $L_z = 0.5$ m, as shown in Fig. 7. The elasticity modulus $E(y,z) = c\exp[\alpha(y,z)]$ of the plate is assumed to be a two-dimensional independent, homogeneous, lognormal random field with mean $\mu_E = 2.0 \times 10^{11}$ N/m^2 and coefficient of variation $v_E = 0.4$; where $c = \mu_E/\sqrt{1+v_E^2}$ and $\alpha(y,z)$ is a zero-mean, homogeneous, Gaussian random field with variance $\sigma_\alpha^2 = \ln(1+v_E^2)$ and covariance function $\Gamma_\alpha(y,z) = \sigma_\alpha^2 e^{(-|y_1-y_2|/b_y)+(-|z_1-z_2|/b_z)}$. b_y and b_z are the correlation parameters at y and z directions, respectively. The thickness of the plate is 1 mm and Poisson's ratio is 0.30. The Karhunen–Loève approximation is employed to discretize the random field $\alpha(y,z)$ into 10 standard Gaussian random variables. Therefore, a total of 10 random variables are involved in this example.

A 10×5 FE mesh of the plate consisting of 50 two-noded solid elements and 303 nodes. The eigensolutions of the covariance function are obtained by solving the integral equation (Eq. (5)) analytically

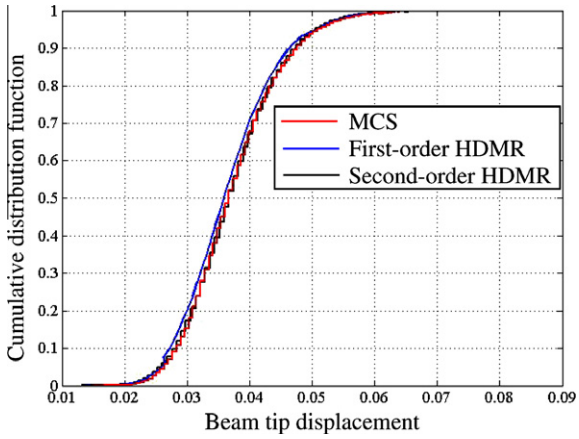

Fig. 6. Cumulative distribution function for beam tip displacement.

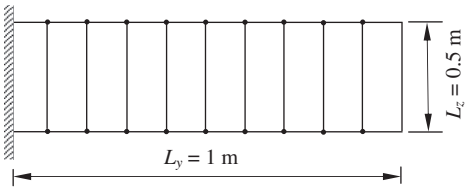

Fig. 7. Cantilever plate.

$$\lambda_i \psi_i(y_2, z_2) = \int_{-b_y/2}^{b_y/2} \int_{-b_z/2}^{b_z/2} \Gamma(y_1, z_1; y_2, z_2) \psi_i(y_1, z_1) dy_1\, dz_1. \tag{28}$$

Substituting the covariance function and assuming the eigensolution is separable in y and z directions, i.e.

$$\psi_i(y_2, z_2) = \psi_i^{(y)}(y_2) \psi_i^{(z)}(z_2) \tag{29}$$

and

$$\lambda_i(y_2, z_2) = \lambda_i^{(y)}(y_2) \lambda_i^{(z)}(z_2). \tag{30}$$

The solution of Eq. (28) reduces to the product of the solutions of two equations of the form

$$\lambda_i^{(y)} \psi_i^{(y)}(y_1) = \int_{-b_y/2}^{b_y/2} \mathrm{e}^{-|y_1 - y_2|/b_y} \psi_i^{(y)}(y_2) dy_2. \tag{31}$$

The solution of this equation, which is the eigensolution of an exponential covariance kernel for a one-dimensional random field, is illustrated in Section 6.1. In the final expression for the eigenfunctions, it should be noted that two functions of the form given by Eq. (31) correspond to each eigenvalue. The second one is obtained from the first one by permuting the subscripts. The final eigenfunctions are given by

$$\psi_k(y, z) = \psi_i^{(y)}(y) \psi_i^{(z)}(z). \tag{32}$$

After obtaining the eigensolutions, the random field is discretized into 10 SRVs, and ten terms K–L expansion is used to generate sample functions of the input random field. The response quantity, which is the natural frequencies of the plate, can be represented by HDMR expansion. Present approach with first- and second-order HDMR approximation and full scale MCS using the commercial FE code (ADINA) [41] are employed for evaluating probabilistic characteristics of natural frequencies of the plate. In all methods, the calculation of the matrix characteristic equation for a given input is equivalent to performing a FE analysis. Therefore, computational efficiency, even for this simple plate model, is a major practical requirement in solving random dynamic problems. For the HDMR-based approach, a value of $n = 7$ was selected.

Fig. 8 shows the first four mode shapes of the cantilever plate when the input is fixed at reference point (mean). Using samples generated from first- and second-order approximations, Table 1 present means, and standard deviations of the four natural frequencies. The tabular results continue to demonstrate the high accuracy of the HDMR-based approach when compared with full scale MCS employing 10,000 FE analyses (samples). In contrast, only 61 and 1681 FE analyses are required by the first- and second-order HDMR with largest errors of 1.82, and 0.48% in calculating means and standard deviations, respectively.

Figs. 9 and 10 show marginal densities of the four natural frequencies by the first- and second-order HDMR approach and the full scale MCS. Due to the computational expense inherent to ADINA analysis, same 10,000 samples generated for verifying the statistics in Table 1 are utilized to develop the histograms in Figs. 9 and 10. However, since the HDMR approximation yields explicit frequency approximations, an arbitrarily large sample size, e.g. 10,000 in this particular example, is selected to perform the embedded Monte Carlo analysis. Agreement between the results of the HDMR approach and the full scale simulation is excellent.

6.3. Plate with circular hole

A rectangular plate subjected to deterministic uniformly distributed load p is considered. In this example, making use of symmetry, only a quarter of the plate is analyzed, as shown in Fig. 11. In this example, performance of the proposed method is examined by considering vector random fields. The elasticity modulus, Poisson's ratio and thickness $E(y,z) = c_1 \exp[\alpha(y,z)]$, $\upsilon(y,z) = c_2 \exp[\beta(y,z)]$ and $t(y,z) = c_3 \exp[\gamma(y,z)]$ of the plate are considered as three two-dimensional independent, homogeneous, lognormal random field. Mean and coefficient of variation of the random fields are $\mu_E = 7.0 \times 10^4$ N/m^2, $\mu_\upsilon = 0.25$, $\mu_E = 0.254$ mm; and $\upsilon_E = 0.4$, $\upsilon_E = 0.3$, $\upsilon_E = 0.6$, respectively. $c_1 = \mu_E/\sqrt{1+\upsilon_E^2}$, $c_2 = \mu_\upsilon/\sqrt{1+\upsilon_\upsilon^2}$, $c_3 = \mu_t/\sqrt{1+\upsilon_t^2}$ and $\alpha(y,z)$, $\beta(y,z)$, $\gamma(y,z)$ are zero-mean, homogeneous, Gaussian random fields with variance $\sigma_\alpha^2 = \ln(1+\upsilon_E^2)$, $\sigma_\beta^2 = \ln(1+\upsilon_\upsilon^2)$, $\sigma_\gamma^2 = \ln(1+\upsilon_t^2)$ and covariance function $\Gamma_\alpha(y,z) = \sigma_\alpha^2 \mathrm{e}^{(-|y_1-y_2|/b_y)+(-|z_1-z_2|/b_z)}$, $\Gamma_\beta(y,z) = \sigma_\beta^2 \mathrm{e}^{(-|y_1-y_2|/b_y)+(-|z_1-z_2|/b_z)}$, $\Gamma_\gamma(y,z) = \sigma_\gamma^2 \mathrm{e}^{(-|y_1-y_2|/b_y)+(-|z_1-z_2|/b_z)}$. b_y and b_z are the correlation parameters at y and z directions,

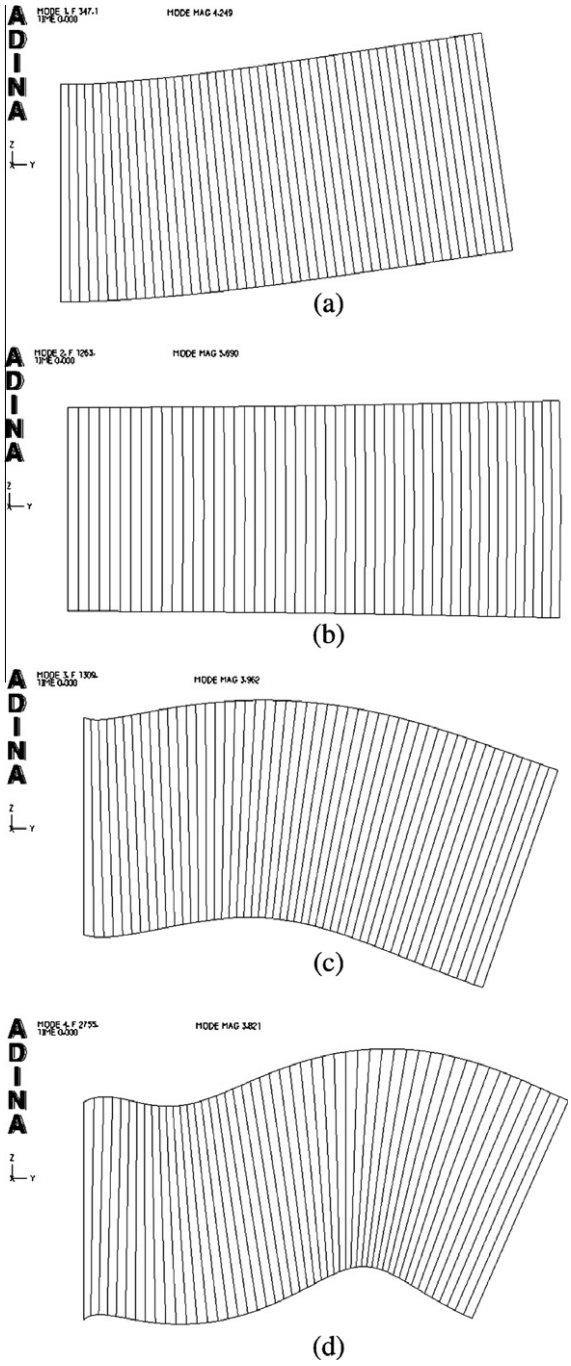

Fig. 8. First four mode shapes of the fixed cantilever plate for mean input.

respectively. The loading is deterministic and $p = 25$ N/mm^2. The plate is discretized into 350 elements in commercial FE code (ADINA) [41].

After obtaining the eigensolutions, the random field is discretized into ten SRVs, and 10 terms K–L expansion is used to generate sample functions of the input random field. The response quantity, which is the vertical displacement at a particular node (Point A), can be represented by HDMR expansion with five ($n = 5$) sample points. Figs. 12 and 13 show the probability distributions obtained from full scale MCS and HDMR with 10 K–L variables. A good agreement is observed between the results from HDMR-based metamodel and full scale MCS (1×10^4 samples).

Compared with the first two response moments obtained using full scale MCS ($m_1 = 7.865 \times 10^{-3}$, $m_2 = 1.219 \times 10^{-4}$) present method using first-order HDMR approximation, overestimates the first two moments by 3.74%

Table 1
Means and standard deviations of first four natural frequencies for the cantilever plate.[a]

Frequency	Mean			Standard deviation		
	First-order HDMR	Second-order HDMR	Monte Carlo	First-order HDMR	Second-order HDMR	Monte Carlo
1	338.15 (−0.51)	336.14 (0.08)	336.42	38.98 (−0.44)	38.75 (0.15)	38.81
2	1200.17 (1.82)	1216.48 (0.49)	1222.42	134.56 (−0.48)	134.02 (−0.07)	133.92
3	1274.76 (−0.61)	1266.88 (0.01)	1267.01	133.39 (−0.44)	132.88 (−0.05)	132.81
4	2690.20 (−0.96)	2668.0 (−0.13)	2664.58	250.98 (−0.22)	250.42 (0.01)	250.44

[a] Parenthetical values represent percentage of relative errors when compared with the full scale MCS.

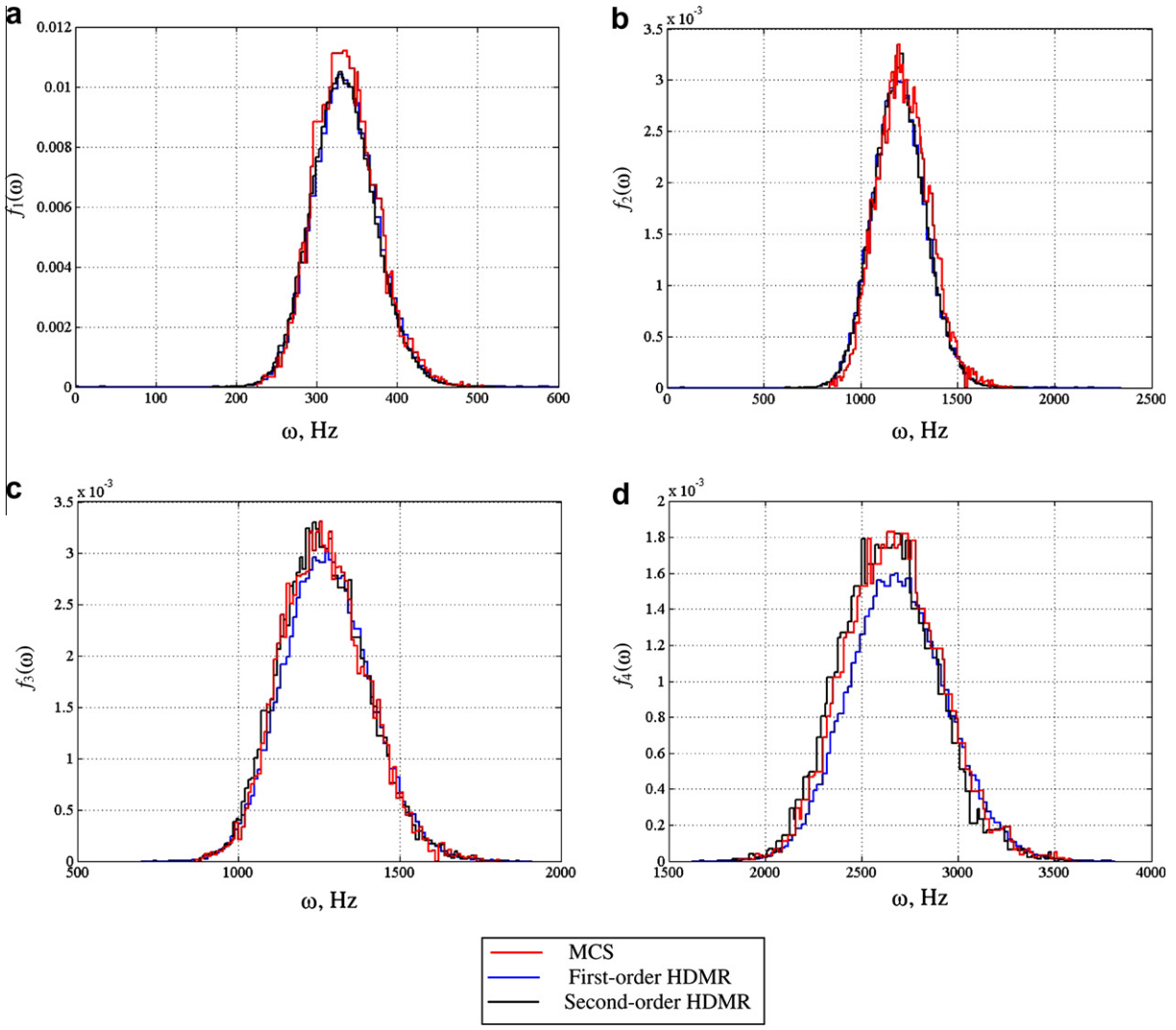

Fig. 9. Probability densities of first four natural frequencies.

($m_1 = 8.159 \times 10^{-3}$) and 39.34% ($m_2 = 7.394 \times 10^{-5}$), respectively, while second-order HDMR approximation, overestimates the first two moments by 0.42% ($m_1 = 7.898 \times 10^{-3}$) and 4.68% ($m_2 = 1.274 \times 10^{-4}$), respectively. However, the present method using first- and second-order HDMR approximation needs 41 and 761 original FE analysis, respectively, while full scale MCS requires 1×10^4 number of original FE calculation. This shows the accuracy and the efficiency (in terms of FE analysis) of the present method using first-order HDMR approximation, direct MCS.

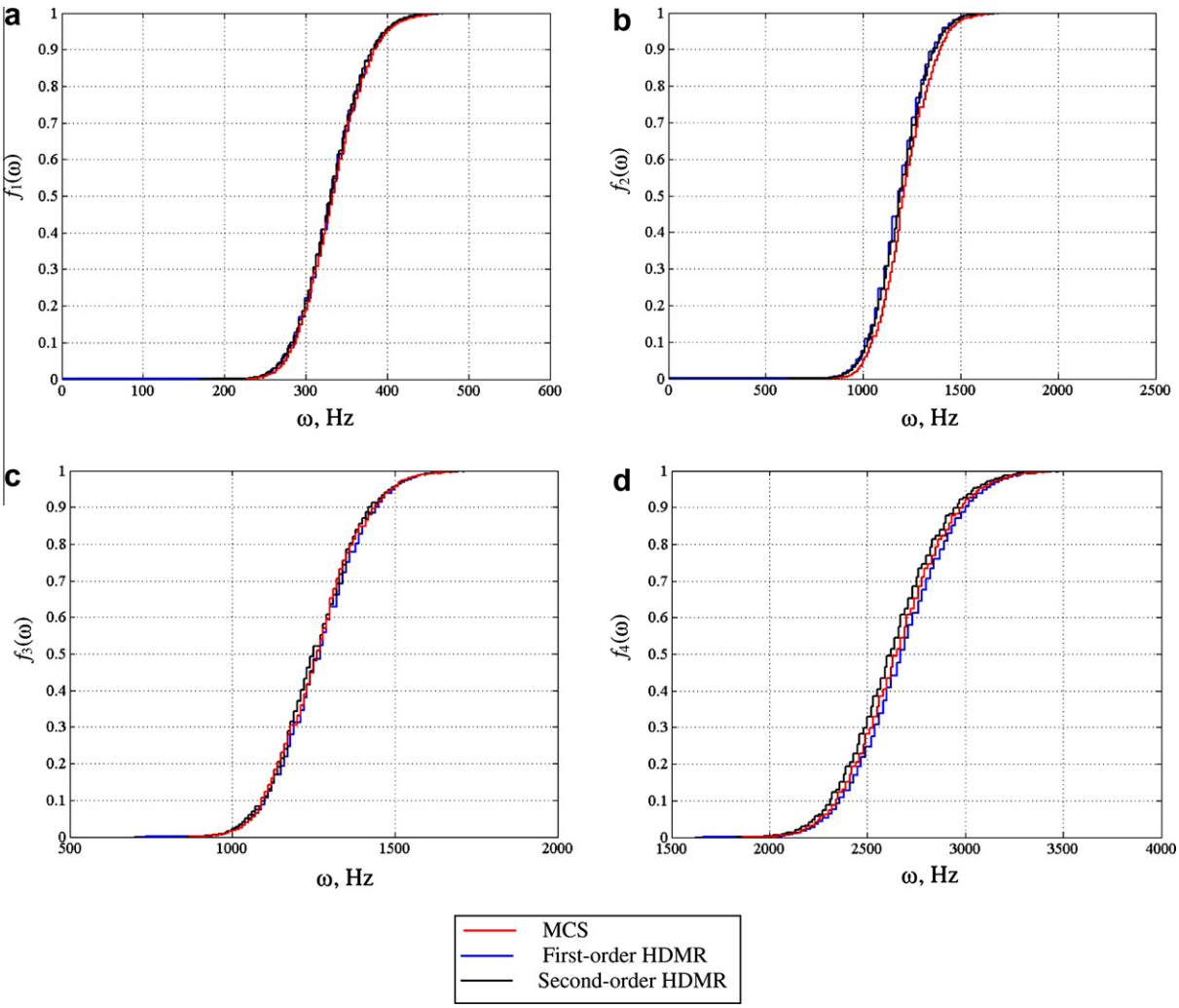

Fig. 10. Cumulative densities of first four natural frequencies.

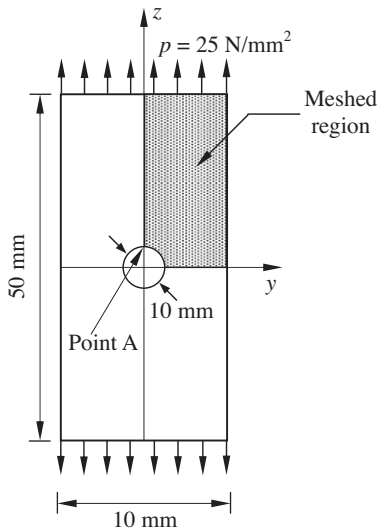

Fig. 11. Rectangular plate with circular hole.

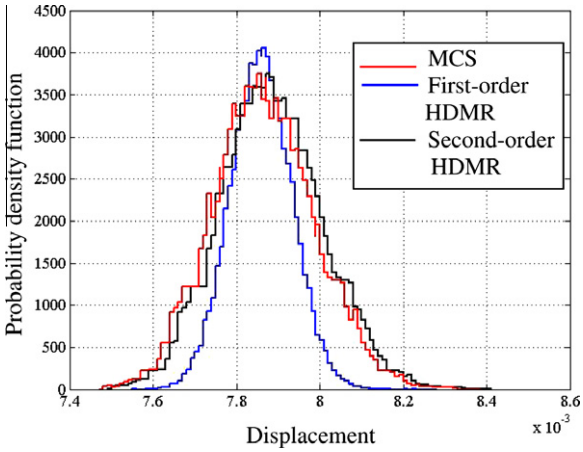

Fig. 12. Probability density function for the vertical displacement at point A of the plate.

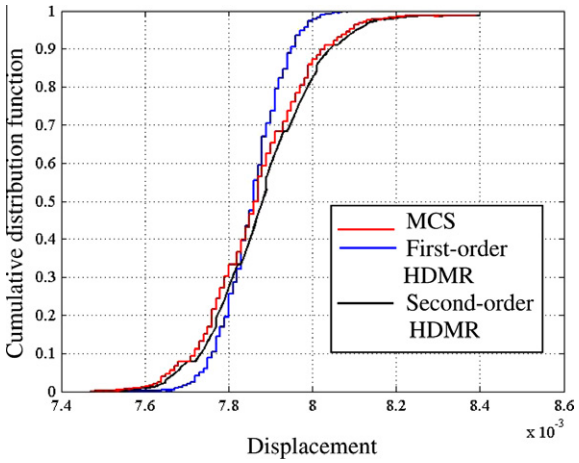

Fig. 13. Cumulative distribution function for the vertical displacement at point A of the plate.

7. Summary and conclusions

This paper presents extended HDMR approach for problems in which physical properties exhibit spatial random variation. The method appears to be efficient, requiring only conditional responses at selected sample points to accurately compute solution statistics. In comparison, full scale MCS may require thousands of realizations or more for converged statistics. Thus the proposed method substantially reduces the computational effort while maintaining the desired accuracy. K–L expansion is required for discretizing the input random field with many terms, which in turn can increase the dimensionality of the problem and thus the computational effort of the SFEM. The curse of dimensionality, which is a problem in other currently available methods, does not arise in the proposed approach. This is because it discretizes the whole problem into a number of subproblems.

Also, the proposed method is independent of the details of structural analysis (in the context of commercial software) as it treats the FE model as a black box. If higher loads introduce nonlinearity in the model response, then the appropriate nonlinear analysis should be used, and the underlying HDMR-based metamodel would automatically be different. Thus the proposed method is applicable to the analysis of linear as well as nonlinear structures, provided the right FE software is used. Good agreements are observed comparing the numerical results between extended HDMR and full scale MCS. However, following observations can be made easily from this article:

Computational effort: HDMR-based approach requires conditional responses at selected sample points and the sample points are chosen along each of the variable axis. It is found in authors' previous work that $n = 5$ or 7 works well for most the problem. Due to this fact, results for $n = 5$ or 7 are used in this paper to construct HDMR-based metamodels.

Handling spatial variability: Unlike local expansion based methods such as perturbation and Neumann expansion methods HDMR can accurately handle random fields with moderate to large coefficients of variations.

8. Discussion and outlook

In this paper, HDMR-based approximation methods are developed in a comprehensive way for structural mechanics problem with random fields. The presented method couples the commercial FE codes and full scale simulation through approximate models. Formally, Eqs. (17) and (18) can be interpreted as higher order response surface for the response field, defined by means of input random field(s). In contrast with usual response surface methods (e.g. polynomial chaos), HDMR approximation allows to define it at any order in a consistent framework. The following notable advantages of the proposed method may be recognized:

- HDMR is a finite sum that contains $2^N - 1$ number of summands and N random variables. In contrast, the polynomial chaos expansion is an infinite series and contains an infinite number of random variables. Therefore, if the component functions in Eq. (9) are convergent, then HDMR approximation provides a convergent solution.
- The terms in the polynomial chaos expansion are organized with respect to the order of polynomials. On the other hand, HDMR is structured with respect to the degree of cooperativity between a finite number of random variables. If a response is highly nonlinear but contains rapidly diminishing cooperative effects of multiple random variables, HDMR approximation is effective. This is due to the fact that, lower-order HDMR approximation can inherently incorporate nonlinear effects in system characteristics. In contrast, many terms are required to be included in the polynomial chaos expansion to capture high nonlinearity.
- The proposed method is independent of the structural analysis (in the context of commercial software) as it treats the FE model as a black box. If the material/geometrical nonlinearity is introduced in the model response, then the appropriate nonlinear analysis should be selected, and the underlying HDMR-based metamodel would automatically be different.
- The amount of computation required for a given problem in SSFEM grows factorially, whereas, in the proposed approach it varies either polynomially.

Note that in all applications found in this paper, only the K–L expansion is used to discretize the input random field(s). The use of other schemes would however be possible and in some case more practical than K–L (for instance when other correlation structures than that with exponential decay are dealt with). Future work will address these issues.

Acknowledgements

RC would like to acknowledge the support of Royal Society through the award of Newton International Fellowship. SA would like to acknowledge the support of UK Engineering and Physical Sciences Research Council (EPSRC) through the award of an Advanced Research Fellowship and The Leverhulme Trust for the award of the Philip Leverhulme Prize.

References

[1] M. Grigoriu, Reduced order models for random functions. Application to stochastic problems, Appl. Math. Model. 33 (1) (2009) 161–175.
[2] Y. Kerboua, A.A. Lakis, M. Thomas, L. Marcouiller, Vibration analysis of rectangular plates coupled with fluid, Appl. Math. Model. 32 (12) (2008) 2570–2586.
[3] Z. Qiu, J. Hu, Two non-probabilistic set-theoretical models to predict the transient vibrations of cross-ply plates with uncertainty, Appl. Math. Model. 32 (12) (2008) 2872–2887.
[4] S. Murugan, D. Harursampath, R. Ganguli, Material uncertainty propagation in helicopter nonlinear aeroelastic response and vibration analysis, AIAA J. 46 (9) (2008) 2332–2344.
[5] M. Chandrashekhar, R. Ganguli, Uncertainty handling in structural damage detection using fuzzy logic and probabilistic simulation, Mech. Syst. Signal Process. 23 (2) (2009) 384–404.
[6] S. Murugan, R. Ganguli, D. Harursampath, Aeroelastic analysis of composite helicopter rotor with random material properties, AIAA J. Aircraft 45 (1) (2008) 306–322.
[7] R. Ghanem, P.D. Spanos, Stochastic Finite Elements: A Spectral Approach, Dover Publications Inc., New York, 2002.
[8] W.K. Liu, T. Belytschko, A. Mani, Random field finite elements, Int. J. Numer. Methods Eng. 23 (10) (1986) 1831–1845.
[9] F. Yamazaki, M. Shinozuka, Neumann expansion for stochastic finite element analysis, J. Eng. Mech. ASCE 114 (8) (1988) 1335–1354.
[10] S. Adhikari, Reliability analysis using parabolic failure surface approximation, J. Eng. Mech. ASCE 130 (12) (2004) 1407–1427.
[11] S. Adhikari, Asymptotic distribution method for structural reliability analysis in high dimensions, Proc. Roy. Soc. London Ser. A 461 (2062) (2005) 3141–3158.
[12] O. Ditlevsen, H.O. Madsen, Structural Reliability Methods, Wiley, Chichester, 1996.
[13] RY. Rubinstein, Simulation and the Monte Carlo Method, Wiley, New York, 1981.
[14] D. Ghiocel, R. Ghanem, Stochastic finite element analysis of seismic soil–structure interaction, J. Eng. Mech. ASCE 128 (1) (2002) 66–77.
[15] R. Chowdhury, B.N. Rao, A.M. Prasad, High dimensional model representation for structural reliability analysis, Commun. Numer. Methods Eng. 25 (4) (2009) 301–337.
[16] R. Chowdhury, B.N. Rao, Assessment of high dimensional model representation techniques for reliability analysis, Probab. Eng. Mech. 24 (1) (2009) 100–115.
[17] R. Chowdhury, B.N. Rao, Hybrid high dimensional model representation for reliability analysis, Comput. Methods Appl. Mech. Eng. 198 (5–8) (2009) 735–765.
[18] B.N. Rao, R. Chowdhury, Enhanced high dimensional model representation for reliability analysis, Int. J. Numer. Methods Eng. 77 (5) (2009) 719–750.
[19] H.L. Van Trees, Detection Estimation and Modulation Theory: Part 1, John Wiley & Sons, New York, 1968.
[20] H. Rabitz, O.F. Alis, J. Shorter, K. Shim, Efficient input–output model representations, Comput. Phys. Commun. 117 (1–2) (1999) 11–20.
[21] H. Rabitz, O.F. Alis, General foundations of high dimensional model representations, J. Math. Chem. 25 (2–3) (1999) 197–233.
[22] S. Huang, S. Mahadevan, R. Rebba, Collocation-based stochastic finite element analysis for random field problems, Probab. Eng. Mech. 22 (2) (2007) 194–205.

[23] B. Sudret, A. Der Kiureghian, Stochastic Finite Element Methods and Reliability: A State-of-the-Art Report, Tech. Rep. UCB/SEMM-2000/08, University of California, Berkley, USA, 2000.
[24] A. Der Kiureghian, J.B. Ke, The stochastic finite element method in structural reliability, Probab. Eng. Mech. 3 (2) (1988) 83–91.
[25] W.K. Liu, T. Belytschko, A. Mani, Probabilistic finite elements for nonlinear structural dynamics, Comput. Methods Appl. Mech. Eng. 56 (1) (1986) 61–86.
[26] G. Matthies, C. Brenner, C. Bucher, C. Guedes Soares, Uncertainties in probabilistic numerical analysis of structures and solids – stochastic finite elements, Struct. Saf. 19 (3) (1997) 283–336.
[27] C.C. Li, A. Der Kiureghian, Optimal discretization of random fields, J. Eng. Mech. ASCE 119 (6) (1993) 1136–1154.
[28] E. Vanmarcke, Random Fields: Analysis and Synthesis, The MIT Press, Cambridge, Massachussets, 1983.
[29] E.H. Vanmarcke, M. Grigoriu, Stochastic finite element analysis of simple beams. J. Eng. Mech., ASCE 109(5) (1083) 1203–1214.
[30] G. Deodatis, The weighted integral method, I: Stochastic stiffness matrix, J. Eng. Mech. ASCE 117 (8) (1991) 1851–1864.
[31] G. Deodatis, M. Shinozuka, The weighted integral method, II : Response variability and reliability, J. Eng. Mech. ASCE 117 (8) (1991) 1865–1877.
[32] T. Takada, Weighted integral method in multidimensional stochastic finite element analysis, Probab. Eng. Mech. 5 (4) (1990) 158–166.
[33] T. Takada, Weighted integral method in stochastic finite element analysis, Probab. Eng. Mech. 5 (3) (1990) 146–156.
[34] J. Zhang, B. Ellingwood, Orthogonal series expansion of random fields in reliability analysis, J. Eng. Mech. ASCE 120 (12) (1994) 2660–2677.
[35] P. Devijver, J. Kittler, Pattern Recognition: A Statistical Approach, Prentice-Hall, London, UK, 1982.
[36] S. Adhikari, Response variability of linear stochastic systems: a general solution using random matrix theory, in: 49th AIAA/ASME/ASCE/AHS/ASC Structures, Structural Dynamics and Materials Conference, Schaumburg, IL, USA, April 2008.
[37] I.M. Sobol, Theorems and examples on high dimensional model representations, Reliabil. Eng. Syst. Safety 79 (2) (2003) 187–193.
[38] G. Li, C. Rosenthal, H. Rabitz, High dimensional model representations, J. Phys. Chem. A 105 (2001) 7765–7777.
[39] P. Lancaster, K. Salkauskas, Curve and Surface Fitting: An Introduction, Academic Press, London, 1986.
[40] S.P. Huang, S.T. Quek, K.K. Phoon, Convergence study of the truncated Karhunen–Loeve expansion for simulation of stochastic processes, Int. J. Numer. Methods Eng. 52 (2001) 1029–1043.
[41] ADINA R&D, Inc., ADINA Theory and Modeling Guide, Report ARD 05 6, 2005.